RESEARCH ARTICLE

Macromolecular Materials and Engineering
Open Access
www.mame-journal.de

Tunable and Biodegradable Poly(Ester Amide)s for Disposable Facemasks

Esteban Alvarez Seoane, Alessandro Cattaneo, Fabien Neuenschwander, Lucien Blanchard, Tatiana Nogueira Matos, Laure Jeandupeux, Gianni Fiorucci, Maryam Tizgadam, Kelly Tran, Pierre-Louis Sciboz, Luce Albergati, Jérôme Charmet,, Roger Marti,,* and Stefan Hengsberger**

The widespread use of disposable facemasks during the COVID-19 pandemic has led to environmental concern due to microplastic pollution. Biodegradable disposable facemasks are a first step to reducing the environmental impact of pandemics. Here, high-performance facemask components based on novel poly(ester amide)s (PEA) grades synthesized from biosourced materials and processed into nonwoven facemask components are presented. PEA-based polymers present an excellent compromise between mechanical performance and biodegradability. Importantly, the properties of the PEA can easily be tuned by changing the ratio of ester and amide, or by varying diol and diacid parts. Seven polymers are synthesized which are optimized for biodegradability and processability. Among them, two grades combines 1) electrospinning process compatibility with 2) full degradation within 35 days, using a normalized biodegradation test. The ultra-thin filters thus developed are evaluated for performance on a custom-made characterization bench. The filters achieve microparticle capture efficiency and air permeability comparable to commercial filters. Another PEA grade is optimized to reach optimal viscothermal properties that made it compatible with solvent-free melt-spinning process as demonstrated with continuous fiber production. Overall, this environmentally friendly solution paves the way for the fabrication of high-performance fibers with excellent biodegradability for the next-generation facemasks.

1. Introduction

During the COVID-19 pandemic, facemasks proved to be an effective way to limit the spread of the virus.[1,2] Commercial medical facemasks are high-tech products which must meet many requirements in terms of hygiene, efficiency, and cost. In general, they are multilayered and include a high-performance filter layer. A recently published communication highlights the environmental impact resulting from disposable facemasks.[3] According to the authors, microplastics originating from standard masks, made of polypropylene and polyethylene, could significantly aggravate global plastic pollution. Other studies also confirm the potential environmental damage that results from improper disposal of facemasks.[4] This ecological issue raises new challenges for the textile industry.

Electrospinning[5,6] is a highly promising technique that was shown to improve facemask performance and reduce the amount of polymer used compared to conventional mask fabrication processes.[7–9] However, even though this fabrication method is more environmentally friendly, the solution is not ideal as it still produces plastic waste. Instead, one of the most promising solutions is to fabricate the facemasks using biodegradable polymers. Biodegradable polymers have received considerable attention for biomedical applications, including for facemasks. Instances of electrospun biodegradable facemasks made of polylactic acid (PLA),[10,11] cellulose,[12,13] chitosan,[14,15] and other materials[16,17] were reported recently. Among them, PLA[10] and poly(butylene succinate)[18] electrospun air filters were shown to exhibit high filtration efficiency and good biodegradability.

Among the biodegradable polymers available, poly(ester amide)s (PEAs) appear promising[10,11] as they harbor the high thermal stability, high elastic modulus, and high tensile strength of polyamides combined with the good degradability of polyesters.[19] Another interesting feature of PEAs is the tunability of their physicochemical properties. This explains why PEAs grades have received a lot of attention for biomedical

E. A. Seoane, T. Nogueira Matos, L. Jeandupeux, G. Fiorucci, J. Charmet, Haute Ecole Arc Ingénierie
HES-SO University of Applied Sciences and Arts of Western Switzerland
Neuchâtel 2000, Switzerland
E-mail: jerome.charmet@he-arc.ch

A. Cattaneo, F. Neuenschwander, L. Blanchard, M. Tizgadam, K. Tran, P.-L. Sciboz, L. Albergati, R. Marti,, S. Hengsberger
Haute Ecole d'Ingénierie et d'Architecture de Fribourg
HES-SO University of Applied Sciences and Arts of Western Switzerland
Fribourg 1700, Switzerland
E-mail: roger.marti@hefr.ch; stefan.hengsberger@hefr.ch

The ORCID identification number(s) for the author(s) of this article can be found under https://doi.org/10.1002/mame.202300375

DOI: 10.1002/mame.202300375

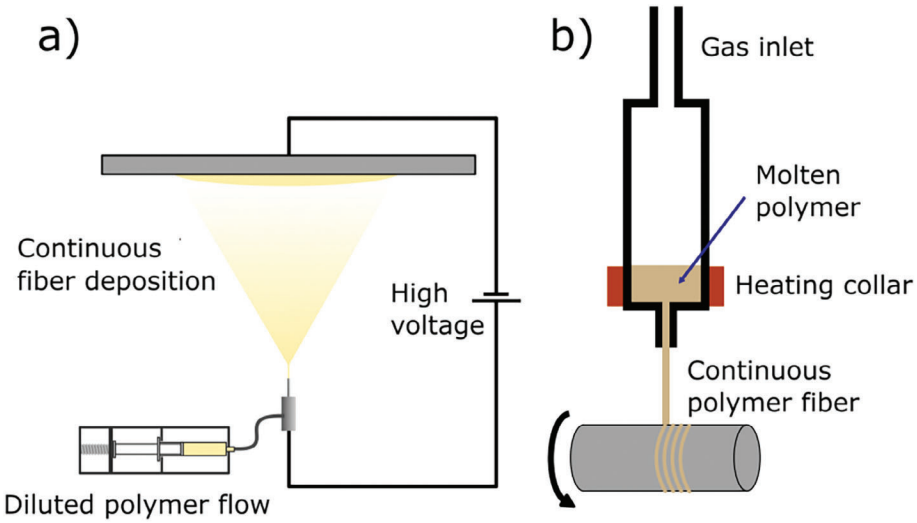

Figure 1. The poly(ester amide)s synthesized and presented in this manuscript were fine-tuned to enable their processing by a) electrospinning and b) melt spinning to allow for the fabrication of high-performance mask filters and fibers compatible with mask outer layers, respectively.

applications.[20] Even though the fabrication of high-grade filters, made by electrospinning of PEA fibers was demonstrated,[19,21] there is no report, to the best of our knowledge, of PEA-based facemasks that demonstrate excellent biodegradability combined with excellent filtration and air permeability.

In this paper, we present and fully characterize novel biodegradable facemasks components made of PEA fibers. In brief, we synthesized seven biosourced poly(ester amide) grades and evaluated them for processing into nonwoven fibers. By varying the ratio of ester and amides and through the tuning of diol and diacid, we systematically optimized PEA grades for biodegradability and processability by electrospinning and melt spinning (**Figure 1**). Selected candidates underwent a normalized biodegradation test, and two polymers were fully degraded in less than 35 days, including one that degraded within 20 days, which is comparable to cellulose. To evaluate the performance of the biodegradable electrospun filters, we realized a custom bench to measure filtration efficacy and air permeability. Compared to commercial filters, our ultra-thin filters demonstrate similar filtration efficiency and air permeability. Finally, we demonstrate that one of our PEA grades is compatible with solvent-free melt-spinning process for the fabrication of outer layers fabric. In particular, we optimized the fabrication process to enable continuous fiber formation on a custom-made rig. Overall, our results pave the way for the development of high-performance biodegradable facemasks based on biosourced PEA.

2. Results

2.1. Polymer Synthesis and Characterization

2.1.1. Polymer Synthesis and Thermal Properties

As shown in **Figure 2a**, a series of PEAs (polymers 1–6) was synthesized by polycondensation from bio-based raw materials such as diols (1,4-butanediol, 1,6-hexanediol, and 1,10-decanediol), diesters (dimethyl adipate and dimethyl 2,5-furandicarboxylate (DMFD)), and an *N,N'*-(butane-1,4-diyl)bis(6-hydroxyhexanamide) referred as 6,4-bisamide-diol building block prepared from 1,4-butanediamine and caprolactone.[22–26] The ratio of unique 6,4-bisamide-diol building block was varied to prepare polymers with different ester-amide content. Gel permeation chromatography (GPC) measurements were performed on the polymers to measure the M_W, M_n, and polydispersity index (PDI) as reported in **Table 1**.

In addition, PEA (polymer 7) based on bis(oxazoline) and sebacic acid was prepared by polyaddition reaction (Figure 2b).[27,28] The first synthesis (polymers 1,2) was performed with 1,4-butanediol at an ester–amide ratio of 50%:50%. This initial selection was done due to the bio-based origin of this diol and the lower boiling point compared to the other candidates (1,6-hexanediol anpolypolyd 1,10-decanediol). The tests performed showed that low molecular weight polymers were synthesized due to sublimation of the oligomers formed during the polycondensation reaction and thus leading to low molecular weight polymers 1 and 2. Polymer 3 synthesized with 1,10-decanediol was straightforward and showed a higher molecular weight in comparison to the first polymers synthesized. However, the cost of this diol encouraged us to select 1,6-hexanediol for further trials and the preparation of polymers 4, 5, and 6.

The summary of the thermal characterization of polymers 1–7 is shown in **Table 2**. The thermograms of the different polymers show a decrease of the glass transition temperature with an increase of the diol aliphatic chain length (Table 2 and Figure S1 in the Supporting Information). This phenomenon is linked to the flexibility of the polymer chains. The longer the aliphatic chain of the diol, the easier it is for the polymer to pass from a glassy state to a rubbery state due to the increased movement possibilities offered by the polymer's chains. A cold crystallization peak can be seen in all the thermograms before melting. The introduction of amide segments prone to hydrogen bonding allows this thermal event in the polymers. As for the T_g, the flexibility of the polymer increases with the length of aliphatic chain of the diol, thus re-

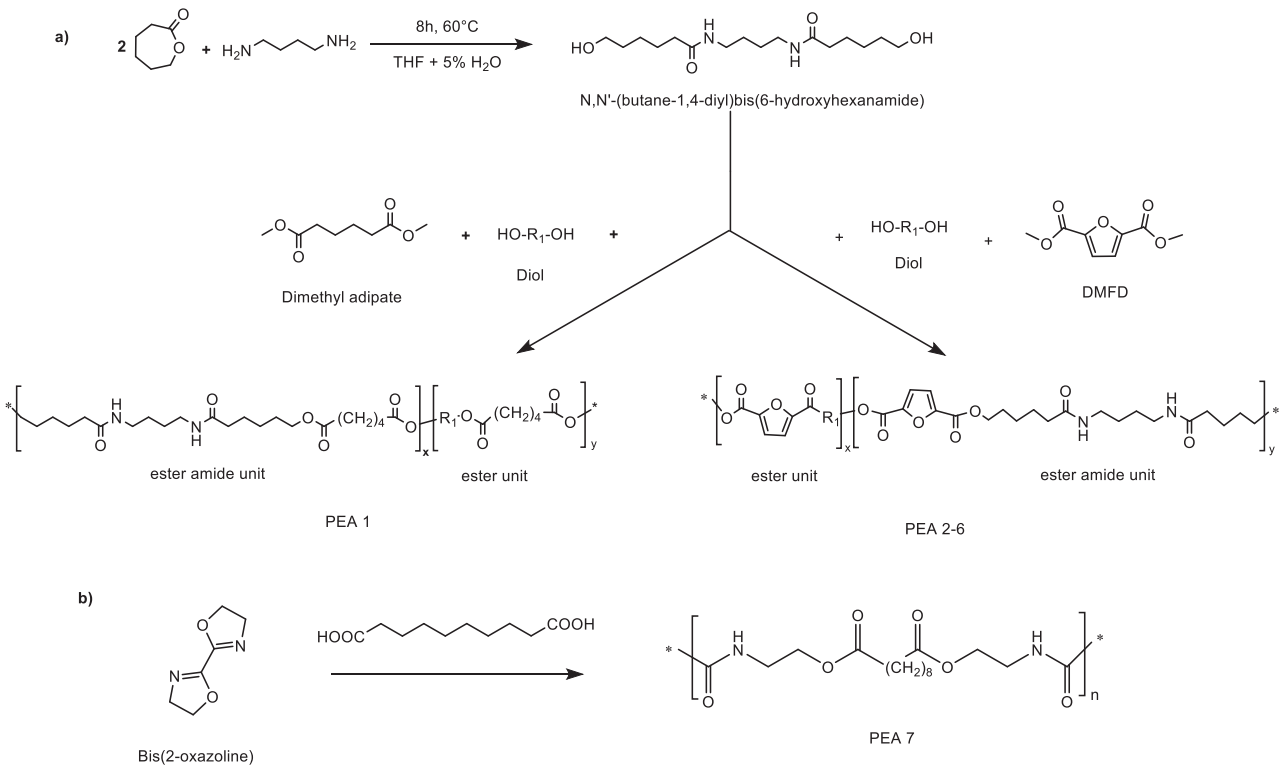

Figure 2. Synthesis of poly(ester amide)s grades. a) Bio-based poly(ester amide)s by polycondensation with dimethyl adipate (PEA 1), and with dimethyl 2,5-furandicarboxylate (PEA 2–6). b) Bis(oxazoline)-based poly(ester amide) 7 by polyaddition.

Table 1. Overview of poly(ester amide)s synthesized by melt polycondensation

Polymer	Diol	Diester	Ester amide ratio	M_W [g mol^{-1}]	M_n [g mol^{-1}]	PDI
1	1,4-butanediol	Dimethyl adipate	50/50	17 700	4800	3.5
2	1,4-butanediol	DMFD	50/50	11 171	5558	2.01
3	1,10-decanediol	DMFD	50/50	36 222	16 078	2.25
4	1,6-hexanediol	DMFD	75/25	51 836	20 346	2.487
Scale-up of 4	1,6-hexanediol	DMFD	75/25	48 957	20 888	2.344
5	1,6-hexanediol	DMFD	50/50	7512	3699	2.031
6	1,6-hexanediol	DMFD	25/75	37 528	17 220	2.179

Table 2. Overview of thermal data (DSC) for the seven polymer grades

Polymer	T_g [°C]	Cold cryst. [°C]	Mp 1 [°C]	Mp 2 [°C]
1	- 38.4	-	73.71	133.3
2	27.5	111.6	134.4	-
3	12.7	71.9	139.7	-
4	18.1	-	119.8	-
5	26.0	105.5	137.5	-
6	27.5	-	157.8	171.4
7	17.8	152.0	172.75	-

ducing the energy needed to pass from an amorphous state to a crystal.[24]

The thermal analysis was also performed on polymers synthesized from 1,6-hexanediol with different ester–amide ratio (Table 2 and Figure S2 in the Supporting Information). From the thermograms, one observes that T_g increases with the amide content from an ester–amide ratio of 75–25 (polymer 4) to the 50–50 (polymer 5). After this increase, the T_g stabilizes at around 27 °C. Another observation is that a cold crystallization is present at the 50–50 ester–amide ratio but not in the other two polymers. Finally, the presence of two distinct melting peaks in the PEA with an ester–amide ratio of 25–75 (polymer 6) indicates the melting of the ester and the amide segments. In the other polymers, the ester melting was not observed.

2.1.2. Solubility Tests and Initial Electrospinning Trials

The polymer solubility was tested in different solvents (Table S1 in the Supporting Information). For the first tests of solubility, the polymers 3, 4, and 6 synthesized from 1,4-butanediol, 1,6-

Table 3. Summary of initial electrospinning tests and conditions

Polymer	Solvent	Conc. [%wt]	Voltage [kV]	Distance [cm]	Flow rate [µL min^{-1}]	Collector speed [rpm]	Result
3	HFIP	12	17	12	21	50	Fibers
4	HFIP	8	17	12	31	50	Fibers
4	Chloroform/phenyl ethanol	10	14	15	5	100	Not continuous filament
4	Chloroform/benzyl alcohol	15	9	15	5	100	Spraying
4	Chloroform/phenyl ethanol	12.5	11	15	35	100	Not continuous filament
4	DCM/benzyl alcohol	13	9	15	35	100	Not continuous filament
4	Chloroform/DCM	6.7	25	15	20	100	Spraying
6	HFIP	10	17	13	21	50	Fibers
6	Chloroform/methanol	6.5	8	5	31	100	Spraying
6	Chloroform/ethanol	6.7	25	15	20	100	Spraying
6	DCM/ethanol	6.7	25	11	35	100	Spraying
6	DCM/benzyl alcohol	6.7	25	11	20	180	Not continuous filament
6	Chloroform/DMC	6.7	25	11	20	180	spraying
6	DCM/phenyl ethanol	6.7	10	15	30	180	Not continuous filament
7	HFIP	11	17	12	30	50	Fibers

hexanediol, and 1,10-decanediol with a 50% of hard segment were chosen. In most cases, the polymers present solubility in alcohols and halogenated solvents and are not soluble in carbonates or *N*-methylmorpholine *N*-Oxyde. The results also show that there is no specific solubility pattern. When mixtures of solvents were used, the results presented even greater variability. Methanol represents an exception as most tests were inconclusive when it was present. The solubility of the polymers is highly dependent on the molecular weight, polar forces, hydrogen bonding, and dispersion forces.[29] Thus, the solubility of polymer has to be evaluated and fine-tuned for each synthesized batch.

From these initial observations, a selection of possible solvents for electrospinning was performed. The initial screening was performed on the polymers synthesized from 1,6-hexanediol and 1,10-decanediol. Polymers produced from 1,4-butanediol were not tested due to low molecular weights. The solvent and electrospinning tests performed are summarized in **Table 3**. High boiling point solvents (dimethylcarbonate (DMC), phenyl-ethanol, benzyl alcohol) were selected due to their nonhazardous nature and for the fact that they are found in nature (fruits) making them potentially bio-based. The problem with these solvents is their low vapor pressure which lowers their evaporation rate compared to solvents such as hexafluoroisopropanol (HFIP) and dichloromethane (DCM). The rapid removal of solvent is important to allow for electrospinning continuous fibers. We also performed solubility tests in binary systems that combine a high boiling point with a low boiling point solvent (methanol, ethanol, DCM, and chloroform). Our idea behind this was to maintain the good solubility provided by the high boiling point solvents, while improving evaporation during electrospinning due to the presence of low boiling point solvent. The results of these tests were mostly electrospraying or gelatinous mixture of solvent and polymer on the collector.

Overall, the tests performed with HFIP showed the best results and enabled the continuous deposition of PEA fibers. This solvent was thus selected for further processing.

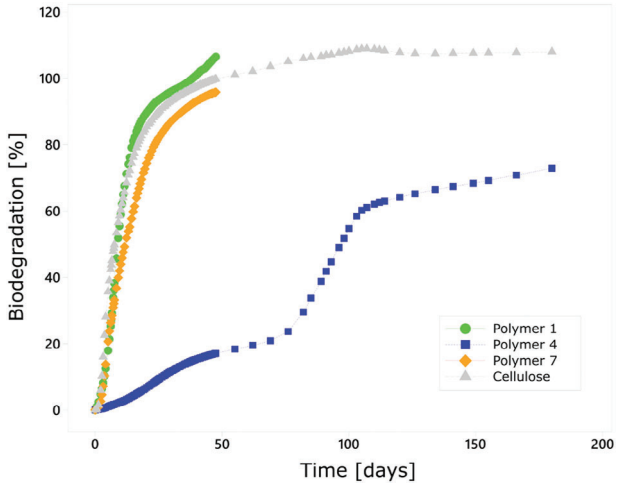

Figure 3. Biodegradability tests based on the norm ISO 14855-1 of three selected poly(ester amide) grades presented in this paper. In brief, the norm involves the measurement of carbon dioxide as a function of time allowing to determine the degradation of the materials in comparison to cellulose reference. The degradation is tested with cellulose as a reference material. A target value of 90% is considered as a total degradation. Polymer 1 achieved a degradation on par with cellulose, with a degradation within 20 days. Polymer 7 was fully degraded after 35 days. Biodegradation was observed for polymer 4, albeit it was slower than for the other two polymers.

2.1.3. Biodegradation Tests

Figure 3 shows the biodegradation results for three PEA grades based on the norm ISO 14855-1.[30] The method reported in the norm involves the measurement of carbon dioxide as a function of time allowing to determine the degradation of the materials in comparison to cellulose reference. A target value of 90% is considered as a total decomposition. Tests showed a rapid degra-

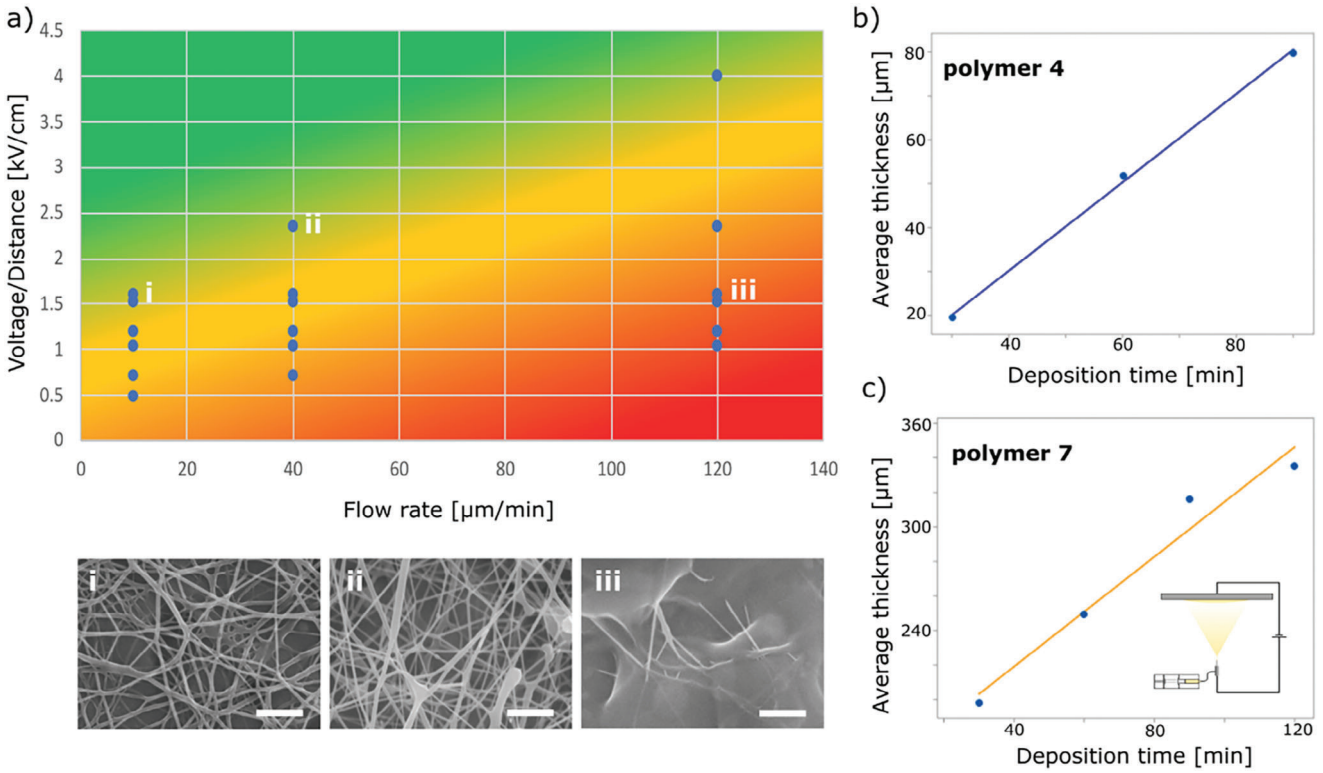

Figure 4. Electrospinning optimization and characterization. a) Fiber quality heatmap as function of the flowrate and the ratio of voltage to distance to collector. Data for 10 wt% solution of polymer 7 in HFIP. Insets show scanning electron micrographs of fibers obtained after deposition under conditions i, ii, and iii. Scale bars indicate 2 µm. Filter thickness as function of the deposition time for b) polymer 4 and c) polymer 7. For these graphs, the electrospinning conditions were 17 kV, 13 cm, and 30 µL min^{-1} for polymer 4 (8%) and 17 kV, 13 cm, and 30 µL min^{-1} for polymer 7 (12.5%). A clear linear correlation is observed between deposition time and polymer layer thickness for each polymer with R^2 value of 99.8% and 96.2% for polymer 4 and 7, respectively.

dation of the two PEA grades polymer 1 and polymer 7. These polymers were completely degraded after less than 35 days, with polymer 1 following the degradation curve of cellulose and a full degradation after about 20 days. The polymer 4 grade presents a slower rate of degradation with a plateau after 45 days followed by an increase between 75 days and 105 days. After 105 days, the polymer slowly continues the degradation until a value of 70% after 180 days. The difference in the degradation is attributed to the different chemical structure and molecular weight of the polymers.

2.2. Electrospinning and Parameter Optimization

Based on the above results, polymer 7, which performed well in the biodegradation test (Figure 3) and produced fibrous materials when dissolved in HFIP during the electrospinning screening tests, was selected to create high-performance filters. Different polymer concentrations were tested for fibers quality by systematically varying the flow rate, the collector distance, and voltage (see *Design* of Experimental Section and Table S2 in the Supporting Information). **Figure** 4a shows the heatmap that represents the quality of the electrospun fibers obtained from 10 wt% solution of polymer 7 in HFIP. The green areas show high-quality, homogenous fibers, while the red areas show poor-quality fibers or electro-spraying. Figure 4a shows that slower flow rate and higher voltage/distance ratio improves the quality of the fibers. In contrast, the heatmap for 12.5 wt% solution of polymer 7 in HFIP (Figure S3 in the Supporting Information) is almost entirely green under the same conditions.

The stark contrast between the results for the 10 and 12.5 wt% highlights the fact that the most important parameter for successful fiber formation is the polymer concentration in the solvent. Indeed, this parameter influences both viscosity and the required time for fiber strands to dry out into solid polymer. This observation is in line with other studies.[31] Then, increasing the voltage and reducing the collector distance also shows a clear improvement of fiber quality, although one should be wary of the influence on process speed and deposition area. For the feed rate, a balance should be found between increased process speed (high feed rate) and better-quality fibers (low feed rates).

2.3. Filter Fabrication and Characterization

2.3.1. Correlation between Deposition Time and Layer

The capture efficiency and the air permeability of the filters depend on fiber size and density, and on the overall filter thickness. The first two parameters were evaluated using scanning electron

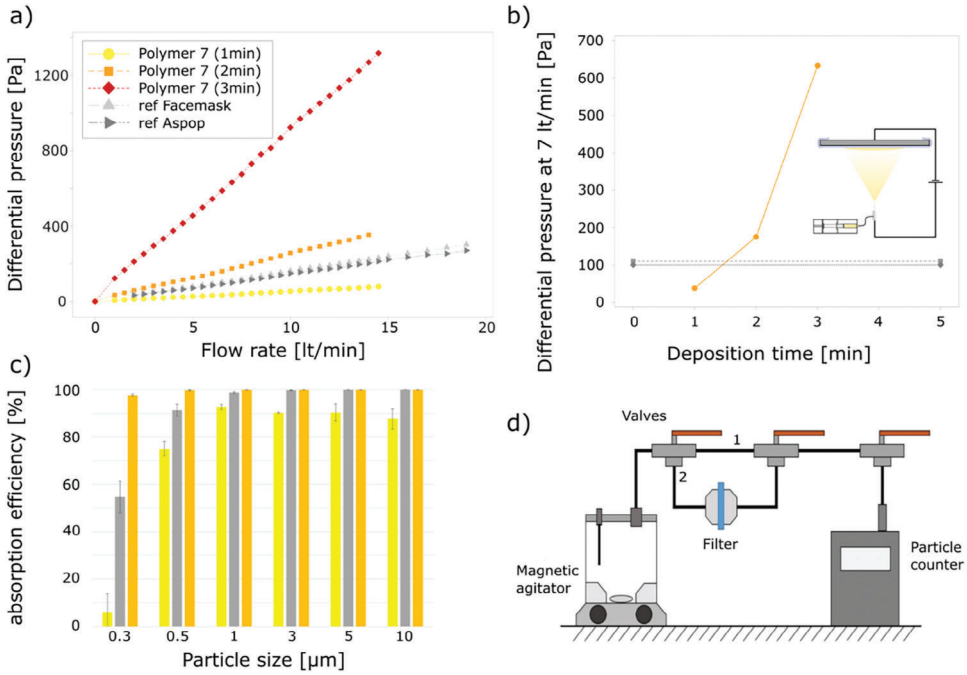

Figure 5. Electrospun filter characterization. a) Analysis of air permeability: Pressure drop for three electrospun filters (polymer 7) with 1, 2, and 3 min electro-spinning deposition time with respect to two commercial facemasks applying different air flow rates (filter and external layer used for all tested samples). b) Optimization of filter electrospinning deposition time for polymer 7. In this figure, the pressure drop values are compared for an air flow rate of 7 L min^{-1} and the air permeability compared to commercial filters (two horizontal lines). c) Absorption test of electrospun filters fabricated with polymer 7 in comparison to the commercial reference « Facemask ». The relative absorption coefficient of microparticles for filters with electrospinning deposition time between 1 and 2 min is in general, respectively, below and above the values obtained using commercial filters. See Figure 5a for color code. d) Principle of the filter performance test: Teflon microparticles are inserted in a magnetic agitator to generate a particle aerosol. A particle counter with an integrated pump analyzes the transmitted microparticles. The particle flow can be alternatively directed through channel 1 for a control of the particle flow intensity and channel 2 to analyze the absorption through the filter. For the measurement of the air permeability, the particle counter is replaced through a vacuum pump with added flowmeter. The differential pressure is measured on both sides of the filter applying a pure air flow.

microscopy (SEM) and for the latter, we used a confocal microscope.

Layer thickness is dependent on feed rate, collector-emitter distance, and significantly on deposition time. Using optimized electrospinning parameters described above, we prepared samples and analyzed them as described in the Experimental Section. It should be noted that when using a static planar collector, the thickness is location dependent, with fibers deposing faster in the center of the pattern than at the edges.[32] Therefore, comparison between samples was systematically made on sections cut at the same collector location as explained in the Experimental Section.

Even though the residual electrical charges buildup on the collected fibers tend to repel the similarly charged jet which limits the maximum thickness of the layer, our data (Figure 4b,c, for polymers 4 and 7, respectively) show that we are still in the linear regime despite the use of deposition times that are longer than needed for the fabrication of our filter (as shown below). However, this experiment shows that we can simply control filter thickness by varying the deposition time.

2.3.2. Filter Performances Measurement

Figure 5d shows a sketch of the characterization bench developed to measure the filtering efficacy of the filters. An optical image of the bench is available in Figure S4 in the Supporting Information. A magnetic agitator is used to create an aerosol of Teflon particles that directly passes to the particle counter (channel 1). Once a stable particle flow intensity is achieved, the particle stream is directed to filter (channel 2) and the resulting particles passing through are counted, thus enabling a differential measurement.

Since the particle detector allows for an independent analysis of 1 and 3 µm particles, two norms (95% absorption of 3 µm particles OR 70% absorption of 1 µm particles) currently in use in Europe (95%/3 µm) and proposed by Swiss hospitals (70%/1 µm)[33] were evaluated.

For the air permeability characterization, the aerosol generator is removed, and the particle counter is replaced by a vacuum pump. An air flow controller (PFM750S-F01-F, Distrelec) and a differential pressure detector (Manometer Testo 512, 0–20hPa) are then added to the circuit. For the analysis of air permeability, the pressure drop across the filter is evaluated. The flow range is between 0 and 14 L min^{-1}.

Varying the deposition time to control filter thickness allowed us to bring both the particle absorption and air permeability closer to market products. The results have allowed to identify an optimal filter deposition time between 1 and 2 min (Figure 5). Since these thin filters are difficult to handle, due to strong electrostatic charging, the electrospinning process was adapted to deposit the filter directly on the outer layer of sheets of com-

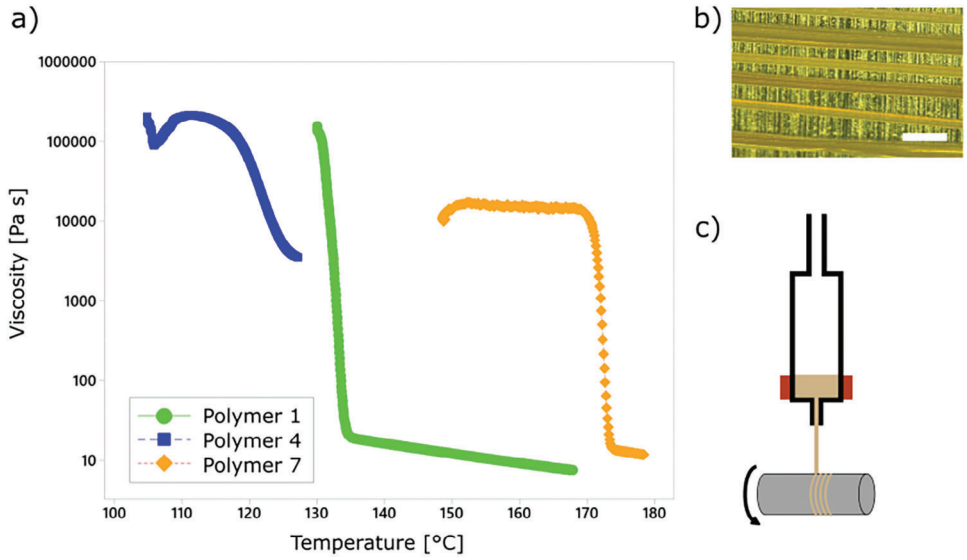

Figure 6. PEA grade optimized for melt-spinning process. a) Viscosity versus temperature for the three PEA grades around the melting point. Polymer 4 shows a smoother variation of viscosity around the melting point in comparison to polymer grades 1 and 7. This explains why the polymer grade 4 is less sensible for temperature fluctuations and better fits for melt spinning. b) Optical micrograph of continuous fibers as obtained by melt spinning the polymer 4. The scale bar corresponds to 250 µm. The used processing temperature was 175 °C with a nitrogen flow of 19.2 L h^{-1} and a collector rotational frequency of $f = 300$ Hz. c) Principle of the melt-spinning equipment. A nitrogen flow pushes the molten polymer through a nozzle and fibers are collected by a rotating cylinder.

mercial facemasks (spun-bound nonwoven polypropylene, supplied by EPSA-Swiss). Therefore, in this case, the measurements of all electrospun and reference samples are made on an outer layer/filter composite. It is noted that even though a potential mechanical mismatch between the layers could lead to delamination, none were observed during our experiments. We attribute this to a combination of strong electrostatic forces and the fact that the electrospun layers are very thin (a few microns).

To evaluate the filter performance, we performed a differential measurement with the outer layer only. The pristine outer layer substrate was tested individually and its influence on the air permeability and filtration was insignificant compared to the filter. Figure 5a shows the air permeability of our filters, based on polymer **7** in comparison with commercial mask references. As expected, the pressure drops increase with filter thickness, for all the flow rates tested. The pressure drops observed for deposition times between 1 and 2 min correspond to the values of the commercial filters. In either case, our filters are within the above-mentioned norm. The particle capture efficiency of the filters is shown in Figure 5c. The filtration performance with a 2 min electrospinning deposition time is better than our reference commercial filter, while the filter fabricated within 1 min exhibits a lower capture efficiency for all particle sizes. Importantly, compared to our reference commercial filter, the electrospun PEA-polymer **7** filter with 2 min deposition time shows a significantly higher absorption rate for both 1 and 3 µm particles while respecting the air permeability norm (we also refer to the discussion for this point). In summary, by controlling the thickness of the filters through deposition time and using the optimum electrospinning deposition parameters, we demonstrated performances comparable with commercial facemasks and with the norms evaluated.

Nanoindentation tests were performed on selected PEA-polymer **7** filters with different deposition time and the two reference facemasks. These tests did not show any significant dependence of the mechanical stiffness on the electrospinning deposition time (not shown), but the electrospun fibers exhibited an elastic modulus twice as large as the commercial PP filters (see details and Figure S5 in the Supporting Information), highlighting again the tunability and excellent mechanical properties of this PEA grade.

2.4. Melt Spinning

Electrospinning is a solution of choice for the fabrication of critical, high-performance filters as shown above and elsewhere in the literature.[34] However, due to its limited throughput, it is not the most appropriate for the fabrication of the outer layer. In this case, more conventional approaches, such as melt spinning, are typically favored, especially since the fibers thus created have a lower constraint in terms of performance efficiency. Therefore, we decided to evaluate the processability of our selected polymers to create nonwoven fabric using melt spinning.

Melt-spinning tests have been successfully applied with polymer 4 as demonstrated by continuous fibers fabrication (**Figure 6b**). The polymer pellets were maintained at a controlled temperature inside the dispenser head and continuous fibers were created and collected by the rotating cylindrical collector (Figure 6c). Due to the speed limitations of the rotating collector (700 rpm), the smallest fiber dimension that could be achieved was 34 µm.

Polymer 4 was the only PEA grade that could be used for melt spinning as no continuous fibers were generated using the two other selected grades. Viscosity versus temperature scans of these

three grades were performed (Figure 6a) to investigate the reason behind the processability of the polymers. The figure highlights two distinct behaviors that differentiate polymer 4 from polymers 1 and 7. The slope of the viscosity around the melting temperature and the final viscosity value reached in the molten state. When heated up to the melting point, polymer 4 shows a lower viscosity drop with temperature compared to the other two PEA grades. Furthermore, over a temperature range of $\Delta T > 16$ K, the viscosity remains above 3000 Pa s in the molten state and is much greater for polymer 4 than for the other two grades. This analysis therefore confirms why polymer 4 is compatible with melt spinning while the other two are not. This is because in the latter cases, small temperature fluctuations can lead to a rupture of the fiber flow.

3. Discussion

In this paper, we present and fully characterize novel PEA-based biodegradable facemask filter components. Several biosourced PEA grades were synthesized, fine-tuned, and evaluated for processing into nonwoven fibers. Normalized biodegradation tests were performed with three selected PEA grades that passed a processability screening test. Two polymers were fully degraded in less than 35 days, including one that degraded as quickly as cellulose, i.e., 20 days.

We then developed electrospun filters that were tested for filtration efficacy and air permeability, using a test bench developed for the occasion. We systematically tested the filtration performance with particles between 0.3 and 10 µm size. Our optimized ultra-thin high-performance filters demonstrate filtration efficiency and air permeability comparable to commercial facemasks.

The filtration efficacy and air permeability of the filters were benchmarked against commercial filters. Disposable facemasks of Type I need to filter 95% of 3 µm particles (norm EN 14683+AC:2019). However, during the COVID-19 pandemic, several Swiss hospitals and medical institutes have requested to add a 70% filtration of 1 µm particle criteria.[35] Commercial filter used as reference herein has been validated using both criteria and the mask used as reference for the filtration test has shown a 95% absorption of 1 µm particles. Furthermore, both commercial masks demonstrated air permeability that was approximately twice better than the normed target value (40 Pa cm^{-2} according to norm EN 14683+AC:2019). Since the performance of our optimized filters is comparable to that of the two reference filters, we conclude that they may respond to the requirements of a normed test.

One further key outcome of our study is the demonstration that the filter material can directly be electrospun on the outer layer of a disposable mask. This ensures a tight contact between the layers and importantly simplifies the production of multilayered systems. In addition, to evaluate the possibility to fabricate the outer layers of the facemasks, we developed a melt-spinning rig capable of continuous fiber fabrication on one of the polymers.

Pandit et al.[19] also claim that biodegradable materials will not only reduce waste but also increase wearing comfort and skin friendliness. Several authors report studies where biosourced and biodegradable filters have been made by electro-spinning, e.g., based on gluten-blended polyvinyl alcohol (PVA)[36] or carbon-blended gluten nanofiber,[37] while other authors propose biopolymers like PVA and PLA[38] for electro-spinning nanofilters. To the best of our knowledge, there are no biodegradable facemasks based on biosourced PEA. PEA is an interesting class of polymers that combines good mechanical properties, biodegradability, and importantly that is amenable to seamless modifications to fine-tune their properties as shown herein.

One open point of this research pertains to the solvent used for electro-spinning, HFIP, that is not a green solvent. Despite comprehensive tests with other solvents like methanol and ethanol and mixtures of HFIP with green solvents, the presented electrospinning results have only been achieved using pure HFIP.

Overall, our results pave the way for the development of high-performance biodegradable facemasks based on biosourced PEA. Future studies, outside of the scope of this manuscript, will address the ideal combination of melt-spinning and electrospinning process to fabricate an entire facemask. The studies will also include water vapor transmission rate and wearing comfort. The potential final costs of a disposable biodegradable facemask will also be evaluated and factors like the upscaled PEA synthesis and a production including an electrospinning step will be considered.

4. Experimental Section

Synthesis of Biodegradable PEAs: *General information*: DMFD was purchased from Apollo Scientific, 1,4-butanediol; 1,6-hexanediol; 1,10-decanediol; DBTO were purchased from Acros Organics. Diethyl ether; absolute alcohol with 5% isopropyl alcohol; tetrahydrofuran with butylated hydroxytoluene stabilizer; methanol, 99% were purchased from Thommen-Furler AG and used without any further purification; titanium (IV) butoxide was purchased from Fluorochem and dissolved in toluene at the desired concentration prior to use.

NMR spectra were recorded with a Bruker 300 Ultrashield spectrometer and referenced against the chemical shift of the residual protio-solvent peak ($CDCl_3$: 7.26 ppm; DMSO-d_6: 2.50 ppm; D_2O: 4.79 ppm) for ^{1}H NMR and the deuterated solvent peak ($CDCl_3$: 77 ppm; DMSO-d_6: 40 ppm) for ^{13}C NMR measurements.

IR spectra were recorded on a Bruker ALPHA in absorption mode between 4000 and 400 cm^{-1} with a resolution of 4 cm^{-1}. Samples were analyzed directly on the diamond crystal without further preparation (not shown).

Differential scanning calorimetry (DSC) measurements were carried with a Mettler DSC 821e. The analyses were conducted under nitrogen in Al 40 µL crucibles with a heating and cooling rate of 10 °C min^{-1}. Method: −70 to 200 °C, 1 min annealing, 200 to −70 °C, 1 min annealing, −70 to 200 °C.

A TGA/SDTA851e (Mettler Toledo) instrument was used to study the thermal stability of the synthesized polymers. To this purpose, 5–10 mg of polymers were placed in a standard aluminum pan and heated under nitrogen from 30 to 800 °C at a heating rate of 10 °C min^{-1}. The first indicator was the temperature for which the weight loss was equal to 5% ($T_{d,5\%}$).

GPC measurements were performed on a Waters 1260 infinity pump, a 1260 Infinity II Refractive Index Detector, a 1260 Infinity II Multisampler, an Acquity APC XT 45, 1.7 µm column an Acquity APC XT 125, 2.5 µm followed by an Acquity APC XT 200, 2.5 µm columns in series at 30 °C. A 10×10^{-3} M solution of sodium triacetate in HFIP was used as eluent at a flow rate of 0.3 mL min^{-1}. The molecular weights were calibrated with polymethylmethacrylate (PMMA) standards on a range between 600 and 2 200 000 Da (PSS Polymer Standards Service, Mainz, Germany).

For the test of polymer solubility, a defined amount of polymer and solvent was charged in a vial and left stirring until dissolution. Solubility was evaluated visually.

Synthesis of PEAs: The 6,4-bisamide-diol building block was synthesized as reported in references.[39,40]

^{1}H NMR signals of 6,4-bisamide-diol (300 MHz; DMSO-d_6, δ): 7.74 (t, J = 5.6 Hz, 1H), 4.39–4.30 (m, 1H), 3.37 (dd, J = 6.4; 4.7 Hz, 2H), 3.00 (q, J = 6.1 Hz, 2H), 2.03 (t, J = 7.4 Hz, 2H), 1.58–1.15 (m, 3H).

Polymers were synthesized following the same procedure that comprised a first step where transesterification of DMFD or dimethyl adipate occurred with the consequent removal of methanol and a second polycondensation step where the polymer chains grew, and the removal of the diol took place. An example of the synthesis of polymer **2** with DMFD and 1,4-butanediol to form a 50% hard segment is reported.[40]

In a 500 mL three-necked round-bottom flask mounted with a distilling bridge and a helical stirrer connected to the system via a magnetic coupling, 58.18 g of DMFD (321.19 mmol, 1 eq.), 50.93 g of building block 6,4-bisamide-diol (97.5% purity, 157.75 mmol, 0.49 eq.), 14.47 g of 1,4-butandiol (160.56 mmol, 0.5 eq.) were introduced and three cycles of argon/vacuum were made to ensure inert atmosphere. The flask was heated to 190 °C using an aluminum heating block (DrySyn) under argon atmosphere. Once the reactants melted, the stirring was enabled at 200 rpm and 4 mL of a 30 mg mL^{-1} stock solution in toluene of titanium *tert*-butoxide (catalyst, 180 mg, 0.52 mmol) was added through a septum. During the esterification, a stream of argon was purged through the reactor to remove methanol and toluene efficiently. Once the distillation ended, the distillation collector was emptied, dried, and re-connected. Then, 4 mL of a 30 mg mL^{-1} stock solution in toluene of titanium *tert*-butoxide (catalyst, 180 mg, 0.52 mmol) was added through a septum.

The temperature was increased to 205 °C, the pressure was reduced to 0.02 mbar for 1.5 h with a high vacuum pump. After this time, the pressure was increased with argon up to atmospheric pressure and 4 mL of a 30 mg mL^{-1} stock solution in toluene of titanium *tert*-butoxide (catalyst, 180 mg, 0.52 mmol) was added through a septum. After reducing the pressure again, the solution was kept for 1.5 h at 205 °C. Then, the temperature was increased to 210 °C for 1.5 h and finally to 215 °C for 1 h. After this time, the formed polymer (lightly brown viscous liquid) was cast on a metal plate to allow solidification.

Synthesis of 2,2′-bis(2-oxazoline): 2,2′-bis(2-oxazoline) was synthesized based on the procedures reported by Wenker[29] and in the patent WO2012066051A2.[42]

Diethyl oxalate (14.6 g, 0.1 mol, 1 eq.) dissolved in 15 mL of ethanol was added for 1 h to a cooled mixture composed of 2-chloroethylamine hydrochloride (23.2 g, 0.2 mol, 2 eq.) and potassium hydroxide (85%, 13.2 g, 0.2 mol, 2 eq.) dissolved in 20 mL of deionized water. The mixture temperature was kept below 20 °C with an ice bath. At the end of the addition, the mixture was stirred for an additional hour at room temperature. The white precipitate was isolated by vacuum filtration, suspended in 40 mL of deionized water, and stirred for 15 min. The suspension was filtered again by vacuum filtration and washed with 15 mL of ethanol. The powder was dried in a vacuum oven at 80 °C and 50 mbar. 16.92 g of *N*,*N*′-bis(2-chloroethyl)oxamide as a fine white powder was obtained (yield: 79%).

m.p.: 203 °C (203 °C)[29]

^{1}H NMR (300 MHz; DMSO-d_6, δ): 8.95 (t, J = 6.3 Hz, 2H, N—H), 3.70 (t, J = 6.3 Hz, 4H, Cl—CH_2), 3.49 (q, J = 6.2 Hz, 4H, N—CH_2)

^{13}C NMR (75 MHz, DMSO-d_6): δ 160.4 (C═O), 43.0 (C—Cl), 41.3 (C—NH)

IR: ν = 3291 cm^{-1} (s), ν = 3067 cm^{-1} (w), ν = 2961 cm^{-1} (w), ν = 2934 cm^{-1} (w), ν = 1655 cm^{-1} (s), ν = 1534 cm^{-1} (s), ν = 1440 cm^{-1} (s), ν = 1362 cm^{-1} (w), ν = 1311 cm^{-1} (m), ν = 1246 cm^{-1} (s), ν = 1185 cm^{-1} (m), ν = 1055 cm^{-1} (m), ν = 933 cm^{-1} (w), ν = 860 cm^{-1} (w), ν = 760 cm^{-1} (m), ν = 652 cm^{-1} (m), ν = 546 cm^{-1} (m).

N,*N*′-bis(2-chloroethyl)oxamide (13.42 g, 63 mmol, 1 eq.) was suspended in 50 mL of methanol containing 8.32 g of potassium hydroxide (85%, 126 mmol, 2 eq.). The mixture was heated to reflux for 1 h. The resulting suspension was filtered by vacuum filtration at 50 °C. The filtrate was concentrated at 50 °C and 200 mbar. When around 40 mL of methanol was removed, the precipitate was filtered off under vacuum and washed with a small volume (about 5 mL) of cold methanol. A second concentration and filtration step was performed on the resulting filtrate with the same parameters. The powder obtained from these two concentrations was dried in a vacuum oven at 60 °C and 100 mbar. 7.05 g of 2,2′-bis(2-oxazoline) as a white crystalline powder was obtained. (Yield: 80%.)

m.p.: 213 °C (213 °C)[29]

^{1}H NMR (300 MHz; D_2O, δ): 4.49 (t, J = 9.9 Hz, 4H, O—CH_2), 4.00 (t, J = 9.9 Hz, 4H, N—CH_2).

^{13}C NMR (75 MHz, D_2O): δ 156.09 (C═O), 69.24 (O—CH_2), 53.73 (N—CH_2)

IR: ν = 3291 cm^{-1} (w), ν = 2940 cm^{-1} (w), ν = 2872 cm^{-1} (w), ν = 1655 cm^{-1} (w), ν = 1617 cm^{-1} (s), ν = 1538 cm^{-1} (w), ν = 1473 cm^{-1} (w), ν = 1385 cm^{-1} (w), ν = 1348 cm^{-1} (w), ν = 1290 cm^{-1} (w), ν = 1253 cm^{-1} (w), ν = 1188 cm^{-1} (w), ν = 1105 cm^{-1} (s), ν = 971 cm^{-1} (m), ν = 913 cm^{-1} (s), ν = 868 cm^{-1} (m), ν = 725 cm^{-1} (w), ν = 653 cm^{-1} (w), ν = 569 cm^{-1} (m).

Synthesis of 2,2′-bis(2-oxazoline)-based PEAs: Bulk polymerizations of PEAs were carried out according to the procedure reported by Wilsens.[43]

Sebacic acid (6.06 g, 30 mmol, 1 eq.) was mixed with 2,2′-bis(2-oxazoline) (4.62 g, 33 mmol, 1.1 eq.) and Irganox 1330 (0.1 g, 1 wt%). The mixture was mixed and heated under nitrogen atmosphere to 195 °C for 2 h, before the viscous polymer was discharged on a Teflon foil.

Aerobic biodegradation of polymers: Polymers 1, 4, and 7 were grounded with Ultra Centrifugal Mill ZM 200 from Retch to a size lower than 800 µm and sent to OWS.[44]

The controlled composting biodegradation test was an optimized simulation of an intensive aerobic composting process where the biodegradability of a test item under dry, aerobic conditions was determined. The inoculum was consisted of stabilized and mature compost derived from the organic fraction of municipal solid waste. The test item was mixed with the inoculum and introduced into static reactor vessels where it was intensively composted under optimum oxygen, temperature, and moisture conditions. During the aerobic biodegradation of organic materials, a mixture of gases (principally carbon dioxide and water) was the final decomposition product while part of the organic material would be assimilated for cell growth. The carbon dioxide production was continuously monitored and integrated to determine the carbon dioxide production rate and the cumulative carbon dioxide production. After determining the carbon content of the test item, the percentage of biodegradation could be calculated as the percentage of solid carbon of the test item, which had been converted to gaseous, mineral C under the form of CO_2.

The tests were performed according to the norm: ISO 14855-1: "Determination of the ultimate aerobic biodegradability of plastic materials under controlled composting conditions—Method by analysis of evolved carbon dioxide (2012), but in singular instead of triplicate."

Fiber Fabrication through Electrospinning of PEA: The Genvolt electrospinning starter kit, composed of a high voltage power supplier (up to 30 kV) and a syringe pump, was used for early screening. Glass syringes with a metallic needle and a rotating collector were used for the experiments.

Polymers were dissolved in a vial at a given concentration (see Table S1 in the Supporting Information, for details) and left stirring with a magnetic stirrer overnight at room temperature. The polymer solution was then filtered on a 0.22 µm filter and loaded into a 10 mL glass syringe. The syringe was put on the syringe pump and the voltage was connected to the needle. The flow of the syringe pump and the collector speed (rpm) were selected, and the tension was then applied. The tension was slowly increased until the apparition of fibers from the tip of the needle. After the process was finished, the aluminum foil was removed from the collector and the tissue composed of polymer fibers was further used for SEM analysis.

Final electrospinning experiments on selected polymers were realized with a 4Spin device using a 21-gauge needle as the single emitter and a fixed rectangular collector. The setup is represented in Figure 1a. PEA grades were dissolved in HFIP with concentrations ranging between 8 and 12.5 wt% for the selected polymers. Fibers were deposited on aluminum foil or commercial mask outer layer, depending on the condition evaluated, on the collector side. Voltage, working distance, and flowrate were

optimized through experimental design, as detailed in the Supporting Information and Table S2.

Using the results from the experimental design, selected solutions were electro-spun with an emitter-collector distance of 13 cm, a voltage of 17 kV, and a feed rate of 30 µL min^{-1}. Samples for filter performance characterization were made by cutting 50 mm wide disks out of the fabric at the point where the fibers were the thickest, as assessed visually. Deposition time and polymer choice were the only variable for filter fabrication and three filters were made for each parameter setup.

Assessment of Fiber Quality through SEM: Quality of electrospun fibers was assessed visually using a JEOL JSM-6400 scanning electron microscope on metalized samples. Even spreads of long uniform fibers were judged of good quality while the presence of polymer beads indicated electro-spraying. Samples of the experimental design were graded from 1 to 6 (Table S2 in the Supporting Information) and sorted onto a heatmap to better represent the influence of the variable parameters (Figure 4 and Figure S3, Supporting Information).

Measurement of Layer Thickness through Confocal Microscopy: The thickness of layers deposited through electrospinning followed a Gaussian distribution with the center of the stream producing a wider fabric than on the sides. In order to get a measurement of thickness, it was important to account for that variability so that different measurements could be compared. This was done by depositing fibers over a silicon wafer partially covered by peelable masks in a fixed position. A confocal microscope (Sensofar S neox) was then used to measure the height differences over a line between the areas where the mask was peeled off. To ascertain the relationship between layer thickness and deposition time, fibers deposited over 30, 60, 90, and 120 min were prepared for PEA 50% and up to 90 min for PEA 25%.

Nanomechanical Tests of Electrospun PEA Fibers and Commercial Masks: Nanoindentation tests of individual filter filaments were performed with an Ultra nanoindenter UNHT (Anton-Paar) equipped with a Berkovich tip. This local probe method was explained in more detail in many publications, e.g.[45] . Briefly, the diamond tip was loaded into the sample and the force was recorded as a function of the displacement. During the loading phase, the material deformed plastically and elastically whereby both contributions could not be distinguished. During the unloading phase, the material recovered elastically, which allowed to determine the elastic modulus and hardness. For these nanomechanical tests, the filter samples were embedded in PMMA and polished. Indentation tests were performed on individual fibers of selected electrospun PEA filters and of the reference commercial facemasks (see below). For each sample, 15 indentation tests were performed with a maximum load of 200 µN. A linear loading rate of 200 µN min^{-1} was applied, followed by 10 s break at maximum load and an unloading applying a rate of 200 µN min^{-1}. The local elastic modulus and hardness of the fiber material were determined using a Poisson's ratio of 0.3.

Rheological Analysis of PEA Polymers: Rheological tests were performed with an Anton Paar MCR702 TwinDrive rotational rheometer. Viscosity versus temperature scans were carried out for selected PEA grades under a nitrogen atmosphere to avoid oxidation. The temperature interval was defined based on the DSC scans (see Table 2). The measured range covered the melting point of the individual PEA and the temperature was varied at 1 °C min^{-1} applying an oscillation frequency of 1 Hz and an imposed 0.8–1% relative deformation.

Custom-Made Filter Test Bench of Air Permeability and Absorption Test: A filter test bench to measure pressure drop and microparticles absorption rate was conceived and realized in-house. The custom-made bench architecture and working principles are presented in detail in the Results Section. Teflon microparticles (polytetrafluoroethylene powder; CAS: 9002-84-0) with particle diameters ranging from 0.3 to 10 µm were used. The number of particles passing through the filters was counted using a particle counter (HPPC6 Particle Counter Plus 8306; Connect 2 Cleanrooms Ltd., Lancaster, UK) with an integrated pump and detection range of 0.3, 0.5 1, 3, 5, and 10 µm particles. Commercial disposable facemasks, Einwegmaske "Facemask," PP, EN 14683:2019+AC:2019 and Aspop Einwegmaske PP EN 14683 Type IIR, validated in terms of particle absorption and air permeability by Kassensturz (October 2020), were used as reference.

Melt-Spinning Tests: A melt-spinning set-up, allowing for solvent-free fabrication of continuous polymer fibers, was fabricated. It was consisted of an extrusion head (Figure 1b and Figure S6 in the Supporting Information) and a rotating cylindrical collector with a maximum speed of 700 rpm. The polymer was melted in the head body, via a heating collar reaching up to 400 °C and pushed through the nozzle using compressed air.

Supporting Information

Supporting Information is available from the Wiley Online Library or from the author.

Acknowledgements

The authors acknowledge funding from HES-SO (Projet Libre, Public Mask). The authors are grateful to C. Csefalvay for SEM and confocal microscopy measurements. The authors are grateful to M. Choain for supplying EPSA Swiss mask components.

Conflict of Interest

The authors declare no conflict of interest.

Data Availability Statement

The data that support the findings of this study are available in the Supporting Information of this article.

Keywords

biodegradable poly(ester amide), continuous fiber production, disposable facemasks, electrospinning, melt spinning, nonwoven facemasks, PEA, tunable polymers

Received: October 17, 2023
Revised: November 30, 2023
Published online:

[1] D. K. Chu, E. A. Akl, S. Duda, K. Solo, S. Yaacoub, H. J. Schünemann, D. K. Chu, E. A. Akl, A. El-Harakeh, A. Bognanni, T. Lotfi, M. Loeb, A. Hajizadeh, A. Bak, A. Izcovich, C. A. Cuello-Garcia, C. Chen, D. J. Harris, E. Borowiack, F. Chamseddine, F. Schünemann, G. P. Morgano, G. E. U. Muti Schünemann, G. Chen, H. Zhao, I. Neumann, J. Chan, J. Khabsa, L. Hneiny, L. Harrison, et al., *Lancet* **2020**, *395*, 1973.
[2] J. Howard, A. Huang, Z. Li, Z. Tufekci, V. Zdimal, H. M. van der Westhuizen, A. von Delft, A. Price, L. Fridman, L. H. Tang, V. Tang, G. L. Watson, C. E. Bax, R. Shaikh, F. Questier, D. Hernandez, L. F. Chu, C. M. Ramirez, A. W. Rimoin, *Proc. Natl. Acad. Sci. U. S. A.* **2021**, *118*, e2014564118.
[3] O. O. Fadare, E. D. Okoffo, *Sci. Total Environ.* **2020**, *737*, 140279.
[4] E. E. Y. Amuah, E. P. Agyemang, P. Dankwa, B. Fei-Baffoe, R. W. Kazapoe, N. B. Douti, *Resour. Conserv. Recycl. Adv.* **2022**, *13*, 200062.
[5] J. Xue, T. Wu, Y. Dai, Y. Xia, *Chem. Rev.* **2019**, *119*, 5298.
[6] S. Agarwal, J. H. Wendorff, A. Greiner, *Polymer* **2008**, *49*, 5603.
[7] F. N. H. Karabulut, G. Höfler, N. A. Chand, G. W. Beckermann, *Polymers* **2021**, *13*, 3257.

[8] A. Cimini, E. Imperi, A. Picano, M. Rossi, *Appl. Mater. Today* **2023**, *32*, 101833.
[9] Y. Yang, Y. Yang, J. Huang, S. Li, Z. Meng, W. Cai, Y. Lai, *Adv. Fiber Mater.* **2023**, *5*, 1505.
[10] S. K. Murase, J. Puiggalí, in *Natural and Synthetic Biomedical Polymers* (Eds: S. G. Kumbar, C. T. Laurencin, M. Deng), Elsevier, New York **2014**, pp. 145.
[11] A. C. Fonseca, M. H. Gil, P. N. Simões, *Prog. Polym. Sci.* **2014**, *39*, 1291.
[12] L. Wang, Y. Gao, J. Xiong, W. Shao, C. Cui, N. Sun, Y. Zhang, S. Chang, P. Han, F. Liu, J. He, *J. Colloid Interface Sci.* **2022**, *606*, 961.
[13] Z. Wang, C. Zhao, Z. Pan, *J. Colloid Interface Sci.* **2015**, *441*, 121.
[14] B. Sun, J. Lin, M. Liu, W. Li, L. Yang, L. Zhang, C. Chen, D. I. Sun, *ACS Sustainable Chem. Eng.* **2022**, *10*, 1644.
[15] R. Balgis, H. Murata, Y. Goi, T. Ogi, K. Okuyama, L. Bao, *Langmuir* **2017**, *33*, 6127.
[16] H. Li, Z. Wang, H. Zhang, Z. Pan, *Polymers* **2018**, *10*, 1085.
[17] W. Pan, J.-P. Wang, X.-B. Sun, X.-X. Wang, J.-Y. Jiang, Z.-G. Zhang, P. Li, C.-H. Qu, Y.-Z. Long, G.-F. Yu, *J. Cleaner Prod.* **2021**, *291*, 125270.
[18] J. Khan, S. A. Momin, M. Mariatti, V. Vilay, M. Todo, *Mater. Res. Express* **2021**, *8*, 112001.
[19] P. Pandit, S. Maity, K. Singha, Annu, M. Uzun, M. Shekh, S. Ahmed, *Cleaner Eng. Technol.* **2021**, *4*, 100218.
[20] S. Choi, H. Jeon, M. Jang, H. Kim, G. Shin, J. M. Koo, M. Lee, H. K. Sung, Y. Eom, H.-S. Yang, J. Jegal, J. Park, D. X. Oh, S. Y. Hwang, *Adv. Sci.* **2021**, *8*, 2003155.
[21] L. J. Del Valle, M. Roa, A. Díaz, M. T. Casas, J. Puiggalí, A. Rodríguez-Galán, *J. Polym. Res.* **2012**, *19*, 9792.
[22] M. Winnacker, B. Rieger, *Polym. Chem.* **2016**, *7*, 7039.
[23] L. Malinová, M. Stolínová, D. Lubasová, L. Martinová, J. Brozek, *Eur. Polym. J.* **2013**, *49*, 3135.
[24] L. Papadopoulos, P. A. Klonos, M. Kluge, A. Zamboulis, Z. Terzopoulou, D. Kourtidou, A. Magaziotis, K. Chrissafis, A. Kyritsis, D. N. Bikiaris, T. Robert, *Polym. Chem.* **2021**, *12*, 5518.
[25] S. Aziz, L. Hosseinzadeh, E. Arkan, A. H. Azandaryani, *Int. J. Polym. Mater. Polym. Biomater.* **2019**, *68*, 639.
[26] P. A. M. Lips, R. Broos, M. J. M. Van Heeringen, P. J. Dijkstra, J. Feijen, *Polymer* **2005**, *46*, 7834.
[27] P. A. M. Lips, I. W. Velthoen, P. J. Dijkstra, M. Wessling, J. Feijen, *Polymer* **2005**, *46*, 9396.
[28] H. R. Stapert, A. M. Bouwens, P. J. Dijkstra, J. Feijen, *Macromol. Chem. Phys.* **1999**, *200*, 1921.
[29] H. Wenker, *J. Am. Chem. Soc.* **1938**, *60*, 2152.
[30] V. Vannaladsaysy, M. Fakhri, J. Khan, M. Mariatti, *Mater. Today: Proc.* **2022**, *66*, 2767.
[31] C. J. Luo, M. Nangrejo, M. Edirisinghe, *Polymer* **2010**, *51*, 1654.
[32] ISO 14855, ISO 14855-1 Determination of the Ultimate Aerobic Biodegradability of Plastic Materials under Controlled Composting Conditions — Method by Analysis of Evolved Carbon Dioxide — Part 1: General Method. 61010–1 © Iec:2001, https://www.iso.org/standard/57902.html (accessed: October 2023).
[33] A. Haider, S. Haider, I.-K. Kang, *Arab. J. Chem.* **2018**, *11*, 1165.
[34] H. I. Ryu, M. S. Koo, S. Kim, S. Kim, Y.-A. Park, S. M. Park, *Sci. Rep.* **2020**, *10*, 20847.
[35] National COVID-19 Science Task Force (NCS-TF), Recommendations on Minimal Specifications for Community Masks and Their Use Summary of Request/Problem.
[36] D. F. Karabulut, *Revolut. Fibres* **2020**, 1, https://www.srf.ch/news/content/download/19070704/file/Empfehlung_Task_Force_Stoffmasken.pdf.
[37] O. Das, R. E. Neisiany, A. J. Capezza, M. S. Hedenqvist, M. Försth, Q. Xu, L. Jiang, D. Ji, S. Ramakrishna, *Sci. Total Environ.* **2020**, *736*, 139611.
[38] S. Aziz, L. Hosseinzadeh, E. Arkan, A. H. Azandaryani, *Int. J. Polym. Mater. Polym. Biomater.* **2019**, *68*, 639.
[39] V. Vannaladsaysy, M. Fakhri, J. Khan, M. Mariatti, *Mater. Today: Proc.* **2022**, *66*, 2767.
[40] L. Blanchard, C. Rader, E. Vanoli, R. Marti, *Chimia* **2020**, *74*, 1024.
[41] C. Rader, C. Weder, R. Marti, *Macromol. Mater. Eng.* **2021**, *306*, 2000668.
[42] R. Strubl, K. Heinemann, WO/2012/066051, **2012**.
[43] C. H. R. M. Wilsens, N. J. M. Wullems, E. Gubbels, Y. Yao, S. Rastogi, B. A. J. Noordover, *Polym. Chem.* **2015**, *6*, 2707.
[44] OWS website, https://normecows.com/ (accessed: September 2023).
[45] S. Hengsberger, G. Leignel, E. V. Du Breuil, C. Cotting, R. Meuwly, J.-M. Dutoit, T. Chappuis, *Chimia* **2019**, *73*, 1039.

